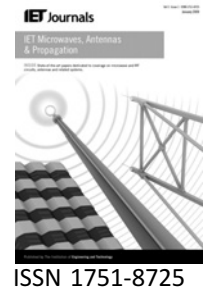


Published in IET Microwaves, Antennas & Propagation  
 Received on 22nd November 2009  
 Revised on 1st April 2010  
 doi: 10.1049/iet-map.2009.0565



# Phase-error performance of multi-focal and non-focal two-dimensional Rotman lens designs

J. Dong<sup>1</sup> A.I. Zaghloul<sup>1,2</sup> R. Rotman<sup>3</sup>

<sup>1</sup>Virginia Polytechnic Institute and State University, Falls Church, VA 22043, USA

<sup>2</sup>US Army Research Laboratory (ARL), Adelphi, MD 20783, USA

<sup>3</sup>IAI Elta Electronics Industries, Ashdod, Israel

E-mail: junweid@gmail.com

**Abstract:** The phase errors of the conventional trifocal Rotman lens and its modified quadrifocal designs could be reduced by adopting a non-focal design scheme. The non-focal design produces minimum average phase errors for all beam ports rather than achieving zero-phase error for only selected focal points. Fundamental models of designing and optimising typical trifocal and quadrifocal planar bootlace lenses are reviewed. Results based on the non-focal design method are compared to the ones from conventional designs, and noticeable improvements demonstrate that the non-focal design scheme is an alternative way of optimising the phase errors for the Rotman lens design. As in referenced papers on multiple-focal designs, the emphasis is on the phase-error analysis and not on experimental verifications.

## 1 Introduction

The Rotman lens [1] has been used in platforms such as radar and satellite communications because of its wideband, wide angle, true time delay (TTD) and multi-beam capabilities. The original Rotman lens was proposed to have three focal points along a two-dimensional (2D) curve determined by solving three simultaneous equations. These equations determine the position of the inner receiving contour and the transmission line path differences, which are the essential parameters of determining the Rotman lens structure. This principle has been applied to the designs of 2D waveguide lenses [1–3] and printed microstrip lenses [4, 5]. Based on the same principle, several modified trifocal Rotman lenses have been investigated [6–8].

Quadrifocal lenses were proposed for 3D lenses that use four simultaneous equations to solve for the position of inner contour and the transmission line length parameters to produce four focal points. Centre plane of the 3D lens has been used to improve the phase performance of the 2D trifocal Rotman lens, as shown in [9].

To implement a Rotman lens with either three or four foci, the first step is to determine the phase centres of the lens by using the path length geometrical equations. The design parameters have to be chosen to achieve satisfactory phase errors for the non-focal beams across the array aperture. Minimising the average phase errors for each of the beams prior to the fabrication is an essential step to guarantee optimal performance of the lens. Port designs [10–12] and amplitude simulations [2, 13, 14] follow.

In this paper, we first review the 2D Rotman lens design based on conventional trifocal and quadrifocal lens theory and summarise various available phase error reduction techniques. Then we show that previous 2D bootlace lens designs lead to a non-focal lens design strategy. This proposed method is robust and has no predefined focal points but emphasises the minimum phase errors for all beams in terms of phase centre positions and transmission line length differences. Similar to the conventional Rotman lens phase evaluation process [1, 6, 7, 9], there is no physical lens implementation presented in this paper, but the assessment will be based on simulations. In this paper,

we intend to show that the minimum-phase-error non-focal lens can be designed using numerical algorithms, capable of incorporating optimisation strategies of most traditional phase-error reduction techniques.

## 2 Rotman lens with focal points

### 2.1 Trifocal lens design

General structure of trifocal Rotman lenses is shown in Fig. 1. Three focal ports indicated by ‘circles’ are predefined on the beam port contour. Energy propagated from beam ports is collected by ports allocated on the receiving port contour. Transmission lines  $W$  then direct the received energy to array elements. Each beam port produces reliable feeding phases and amplitudes for the array elements. When beam port switches, different phases and amplitudes are generated along the phased array, achieving directional scan patterns. Note that the receiving port contour ( $X, Y$ ) and transmission line lengths  $W$  are the undetermined parameters. Hence, trifocal lens theory contains three simultaneous equations to solve these parameters. Assume that the relative permittivity in the medium between beam and receiving ports is  $\epsilon_r$ , and  $\epsilon_c$  is the relative permittivity of transmission line medium.  $Y_3$  is the  $y$ -coordinate of the radiating array element,  $\Psi_a$  is the desired scan angle for focal beam angle  $a$  and  $F_iP$  stands for the distance from the foci to the inner receiving contour that is a function of contour coordinate ( $X, Y$ ). The unknowns  $X, Y$  and  $W - W_0$  are determined by simultaneous equations in

$$\begin{cases} F_1P\sqrt{\epsilon_r} + W\sqrt{\epsilon_c} = f_1\sqrt{\epsilon_r} + W_0\sqrt{\epsilon_c} \\ F_2P\sqrt{\epsilon_r} + W\sqrt{\epsilon_c} + Y_3 \sin(\psi_\alpha) = f_2\sqrt{\epsilon_r} + W_0\sqrt{\epsilon_c} \\ F_3P\sqrt{\epsilon_r} + W\sqrt{\epsilon_c} - Y_3 \sin(\psi_\alpha) = f_2\sqrt{\epsilon_r} + W_0\sqrt{\epsilon_c} \end{cases} \quad (1)$$

In practical designs, along the beam contour, more than three beam ports are usually required to produce multiple scans. Perfect phases are not guaranteed for beams generated from beam ports other than the foci. A couple of phase-error reduction techniques have been proposed by previous

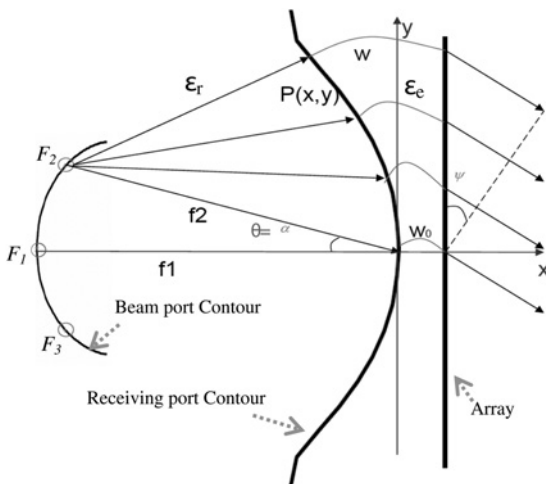


Figure 1 Trifocal Rotman lens design scheme

researchers. First, in the original Rotman’s paper [1], it was found that the ratio between off-axis focal length  $f_2$  and on-axis focal length  $f_1$  greatly affects the phase performance of the non-focal ports, hence the fundamental phase-error reduction method deals with techniques altering this ratio. It was called  $g$  factor in [1], and  $\beta$  factor in [7], with relationship of  $\beta = 1/g$ . Second, techniques involving altering the beam contour, for example, from circular to elliptical, have been introduced in [6, 7]. Third, as shown in Fig. 1, each beam port phase centre has referred to one subtended angle  $\theta$ . In the original Rotman lens model [1], subtended angle is always equal to the scan angle  $\Psi$ . Researchers in [6–8] proved that subtended angle  $\theta$  can be different from scan angle  $\Psi$ , by applying which, it achieved a flexibility of designing more compact beam region for the same scan region, as well as resulting in phase-error reductions.

### 2.2 Quadrufocal lens design

The quadrufocal lens was proposed in designing 3D microwave lens [15]. In the original design, beam ports along 2D curved beam contour were used to feed receiving ports allocated on a 3D curved surface, which are followed by transmission lines directing energy to the output planar phased array. 2D microwave lens is achieved by considering the centre plain of the 3D lens containing the beam contour, as indicated in Fig. 2. Because the 3D model involves four undetermined parameters that are the receiving port position ( $X, Y, Z$ ) and transmission line length  $W$ , it allows four equations, hence four ideal focal points. Similar to trifocal lens, permittivities for centre region and transmission line regions are assumed to be  $\epsilon_r$  and  $\epsilon_c$ . Equations because of the foci path length equality are given in

$$\begin{cases} F_1P\sqrt{\epsilon_r} + W\sqrt{\epsilon_c} + Y_3 \sin \alpha = F_1O\sqrt{\epsilon_r} + W_0\sqrt{\epsilon_c} \\ F_2P\sqrt{\epsilon_r} + W\sqrt{\epsilon_c} + Y_3 \sin \beta = F_2O\sqrt{\epsilon_r} + W_0\sqrt{\epsilon_c} \\ F_3P\sqrt{\epsilon_r} + W\sqrt{\epsilon_c} - Y_3 \sin \alpha = F_3O\sqrt{\epsilon_r} + W_0\sqrt{\epsilon_c} \\ F_4P\sqrt{\epsilon_r} + W\sqrt{\epsilon_c} - Y_3 \sin \beta = F_4O\sqrt{\epsilon_r} + W_0\sqrt{\epsilon_c} \end{cases} \quad (2)$$

where  $\pm \alpha$  and  $\pm \beta$  are values for the four focal subtended angles, as shown in Fig. 2,  $F_iP$  is the physical length

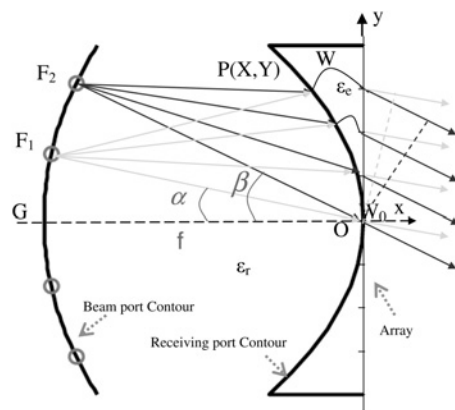


Figure 2 2D quadrufocal lens design scheme

between the  $i$ th beam port and receiving port  $P$  that is function of  $X$  and  $Y$  ( $Z=0$ ),  $Y_3$  is the exterior array element coordinate in  $y$  axis,  $W$  is the transmission line length and  $F_iO = GO = f$ .

In contrast to trifocal lens, four focal ports are formulated on the beam contour, but ports allocated on the non-focal points consequently produce phase errors. Previous work in [9] initially designed a planar quadrifocal lens based on circular beam contour, and conducted phase-error reduction by beam contour perturbation. Note that, different from the trifocal lens, because of the constraint  $F_iO = GO = f$  in initial simultaneous equations' formulation, the quadrifocal lens does not have the flexibility to conduct phase optimisation by adjusting ratio between off-axis focal lengths, as described in [9]. However, one can still migrate optimisation methods of the traditional trifocal lens as adopted in [6–8] into the quadrifocal lens design.

### 3 Non-focal lens design

As described above, the phase errors have become intrinsic characteristics in the bootlace lens design. In realistic environments, to produce multiple beams, more ports in the focal region are expected to lie on the beam contour, as indicated in Fig. 3. In the previous sections' tri- and quadrifocal lens designs, the inner receiver contour and transmission lines are totally determined by the initial focal point parameters, as depicted by equations (1) and (2). Beams produced by these focal ports are theoretically perfect. However, phase errors occur on the non-focal port beams, and optimising these errors become a prime target. As indicated in the previous section, the focal lens optimisation methods are limited in altering non-focal port position, for example, by changing the eccentricity of the ellipse [7] or beam port perturbation [9], and changing the non-focal port scan angle, for example, phase-error reduction method in [6]. There is no unified phase-error reduction method. Besides, each of the aforementioned methods involves complicated lens re-formulations. To choose the best solution, one usually solves trifocal and

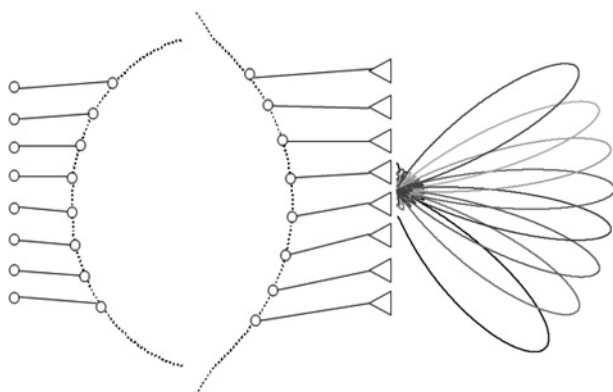


**Figure 3** More beam ports on the focal points are usually expected to occupy the beam contour in realistic design

quadrifocal equations and conduct complicated and separate simulations based on different methods. It is realised that, since the final objective in practice is to minimise the phase errors for all beam ports, instead of constraining limited number of ideal focal points, why not allow introducing perturbations to both beam and inner receiving port contours, transmission lines and even scan angles at the same time. In this sense, conditions for perfect focal points are no longer enforced, and the phase-error performance essentially becomes a function of design variables, with phase-error minimisation achieved in a single optimisation process, as indicated in Fig. 4.

Two tasks are considered in order to design the non-focal lens, one is to build reasonable objective function that describes the general performance of the phase errors for all beam ports, and the other is to seek correct and applicable numerical toolset in optimising the objective function.

Suppose there are  $N$  beam ports and  $M$  inner receiving ports, as shown in Fig. 4. Define  $(x_i, y_i)$  as the coordinates of the  $i$ th beam port with subtended angle at the receiving array centre of  $\alpha_i$ , and  $(x_j, y_j)$  as the  $j$ th receiving port position, with  $w_j$  as the transmission line length reference to transmission line length of the centre receiving port.  $Y_j$  is the  $j$ th phased array element height and  $\Psi_i$  is the radiation angle resulting from the  $i$ th beam port excitation. The lens region and transmission line have dielectric constants of  $\epsilon_r$  and  $\epsilon_c$ , respectively. Given maximum scan angle as  $\pm\Psi_m$  and the maximum subtended angle as  $\alpha_m$ , without losing generality, we can solve

subtended angle increment

$$|\alpha_{i+1} - \alpha_i| = 2\alpha_m/N \quad (1 \leq i < N) \quad (3)$$

scan angle increment

$$|\Psi_{i+1} - \Psi_i| = 2\Psi_m/N \quad (1 \leq i < N) \quad (4)$$

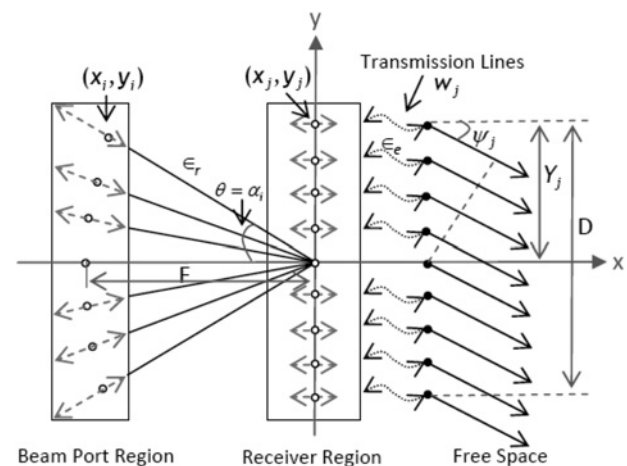


**Figure 4** 2D non-focal lens design scheme

array element spacing

$$|Y_{j+1} - Y_j| = D/M \quad (1 \leq j < M) \quad (5)$$

Other pre-determined parameters suggested include:

$y_j$ :  $y$  coordinate of the  $j$ th receiving port, with typical value of  $Y_j$ ;

$y_i$ :  $y$  coordinate of the  $i$ th beam port, which is equal to  $(x_i^* \tan \alpha_i)$ .

Electrical path length of the  $i$ th beam port to the middle array element phase front is

$$L1 = \sqrt{\epsilon_r} \sqrt{x_i^2 + y_i^2} \quad (6)$$

As shown in Fig. 4, the  $i$ th beam port phase centre to the  $j$ th array element phase front electrical length is

$$L2 = \sqrt{\epsilon_r} \sqrt{(x_i - x_j)^2 + (x_i \tan \alpha_i - y_j)^2} + \sqrt{\epsilon_c} w_j + Y_j \sin(\psi_i) \quad (7)$$

The difference between (6) and (7) gives the theoretical phase error for the  $i$ th beam port excitation. A function relating all phase errors for all beam ports reflects the phase performance, which is defined in (8) as

$$f(x_i, x_j, \alpha_i, \psi_i, \epsilon_r, \epsilon_c, w_j) = \sum_{i=1}^N \sum_{j=1}^M |L2 - L1| \quad (8)$$

Defining the  $F/D$  for lens design is important, because optimisations based on different  $F/D$  values are basically saturated at different phase-error levels, as shown in [15]. This also implies that lens designed using different methods should only compare with one another under the scenario of the same  $F/D$  value. In non-focal lens design, it is suggested to fix centre beam port and middle inner receiver port positions. In this way,  $F$  is constant value and  $r = F/D$  still holds. The total number of each variable, such as  $x_i$  and  $x_j$ , in (8) is  $N - 1$  and  $M - 1$ , respectively.

Parameters  $\alpha_i, \Psi_i$  are usually assigned by relations (3)–(5),  $\epsilon_r$  and  $\epsilon_c$  can be chosen according to model requirement and material availability. As a result, the optimisation of lens phase performance has been transferred to function (8) minimisation in terms of variables  $x_i, x_j$  and  $w_j$ , as given in (9)

$$\min(f) \propto \{x_i, x_j, w_j\} \quad (9)$$

Equation (9) is an  $N + 2M - 3$  dimension global minimisation problem. The objective function  $f$  is addressed in (8). Numerical methods such as genetic algorithms (GA) [16] and Dong Su Zheng algorithms (DSZA) [17] can be adopted to treat such functions. Both algorithms randomly

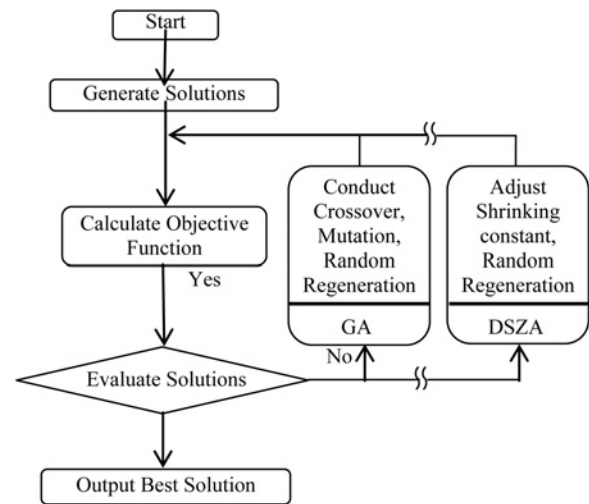


Figure 5 Function optimisation algorithms flowchart

generate finite number of solutions in a form of  $\{x_i, x_j, w_j\}$  and have them weighted by their objective functions; the inferior solutions can be evolved by operations such as mutation or regeneration and so on. In this way, each new loop always passes superior solutions into the next evolution until stable optimum results are produced. The flowchart of such algorithms in principle is shown in Fig. 5, and it is noticed that both methods apply stochastic evolutionary search techniques in optimising the functions.

In traditional focal lens design and optimisation process, the geometry parameters are determined by electrical path equations, and phase-error reductions are conducted separately by single parameter iteration. Differently, the non-focal lens design method does not require focal point constraints to solve geometry equations. It simply combines design freedoms in one phase-error presentation, as shown in (8), conducting numerical process by treating geometry parameters and optimisation factors simultaneously. During the algorithm initialisation, one can preset certain constraints on chosen factors and conduct flexible optimisation on the others. For instance, traditional method of  $\alpha_i < \Psi_i$  can still be applied to design small beam contour lens. A new parameter such as  $\epsilon_r$  is also allowed to involve material property in optimisation during microstrip lens designs. The non-focal lens method is conceptually simple, nevertheless, it requires using numerical optimisation algorithms.

## 4 Comparison and discussion

We now present a design example of a non-focal Rotman lens that minimises the phase error over the array aperture by using the GAs. The lens parameters are based on the ones in quadrifocal lens design [9], and  $F/D$  for each lens is 1. Maximum phase errors normalised to  $F$  against the half-plane subtended/scan angles are compared to the trifocal and quadrifocal lens designs, as shown in Fig. 6. It is noticeable that there are ideal focal points at 0 and 23° for the trifocal lens and at 11 and 25° for the quadrifocal

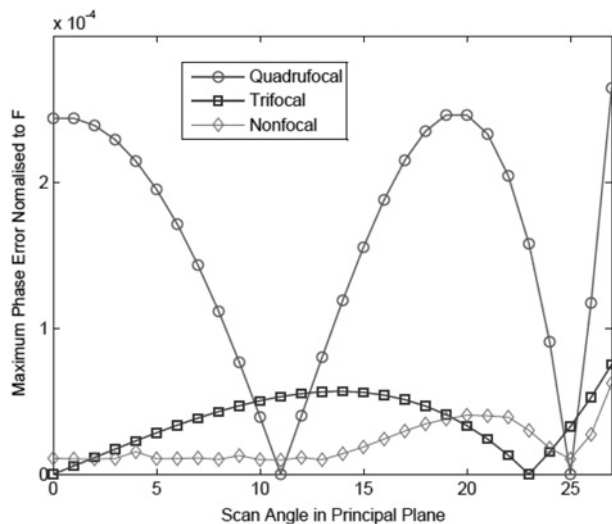


**Figure 6** Comparison between non-focal lens and multiple-focal Rotman lens,  $r = 1$

lens. Although the proposed GA result does not have any perfect focal points, the maximum phase errors for most ports are lower than tri- and quadrifocal lenses, demonstrating that a relatively optimal phase performance is achieved.

The maximum phase errors have been adopted to perform the minimisation during the genetic optimisations, as depicted in Fig. 6. To evaluate the phase performance across the aperture, Figs. 7 and 8 represent the typical phase distributions across the array aperture that consists of 21 uniform spaced elements for the trifocal lens and the non-focal lens at beam port excitations of  $\alpha_i = 10^\circ$  and  $25^\circ$ , respectively. It is observable that the highest phase errors of the trifocal lens occur at the edge receiving ports, whereas the ones of the non-focal lens take place relatively at the centre ports. Although the non-focal lens exhibits higher errors along a few centre ports, on average low-phase errors have been well maintained across the array aperture.

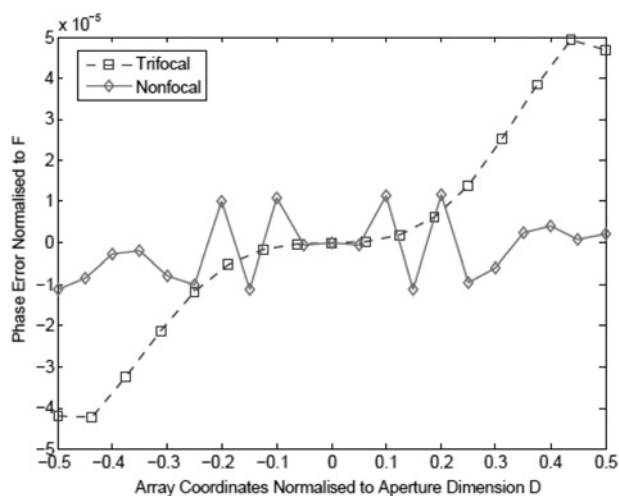


**Figure 7** Phase errors across array aperture of trifocal and non-focal lenses for beam excitation at  $\alpha_i = 10^\circ$

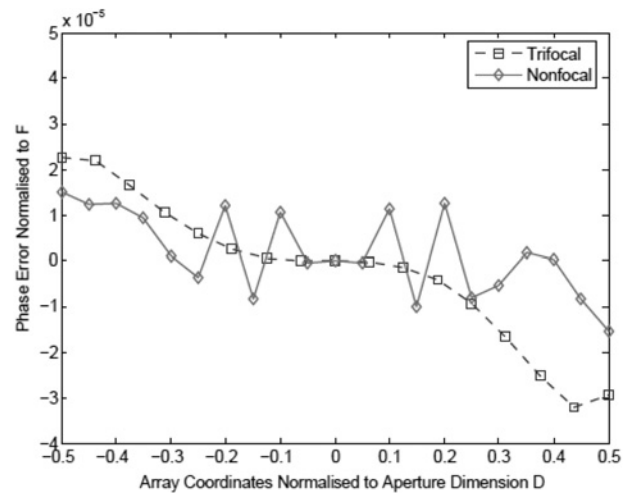


**Figure 8** Phase errors across array aperture of trifocal and non-focal lenses for beam excitation at  $\alpha_i = 25^\circ$

The microwave lens is considered as a TTD structure, hence the phase factors are conventionally normalised to certain geometry dimension on the lens, such as centre 'focal length'  $F$ . In practical design, for different aperture array size and frequency of operation, the phase errors can be viewed from different perspectives, for instance, errors in degrees  $\Delta\varphi_d$ . This relationship is shown in (10), where  $\Delta\varphi_n$  is the phase error normalised to  $F$

$$\Delta\varphi_d = \frac{360F\Delta\varphi_n}{\lambda} = 360r\Delta\varphi_n \frac{D}{\lambda} \quad (10)$$

As indicated in (10), as the aperture in wavelength increases, the effective phase errors in degrees increase. The non-focal lens phase-error reduction becomes significant when feeding large aperture array. This can be practically important by viewing the Rotman lens development trend. In recent years, such device has been proposed in photonic beam forming [18] and extremely high-frequency (EHF) sensor designs [19]. As the frequency increases, the applications may require extremely narrow beams. The required number of array elements may reach hundreds, for example in [20], the number of elements for the imaging system is 130. To illustrate the pattern difference between non-focal and focal lenses for large aperture array, we take the maximum phase errors achieved in Fig. 6 as phase deviations. Given aperture size of  $75\lambda$ , the array factors with uniform illumination for quadrifocal and non-focal lens of zero-degree-beam-port excitations are demonstrated in Fig. 9. The non-focal lens has resulted in lower side lobes than the quadrifocal lens because of its low-phase-error property possessed. In the side lobe region, amplitude improvements of 6 dB are observed. In communication systems, this could typically contribute to lower noise levels.

This paper focuses on a theoretical study, and the examples shown above have addressed such aspect. The following remarks deal with computational and practical issues. First, the convergence time of the global optimisation algorithms

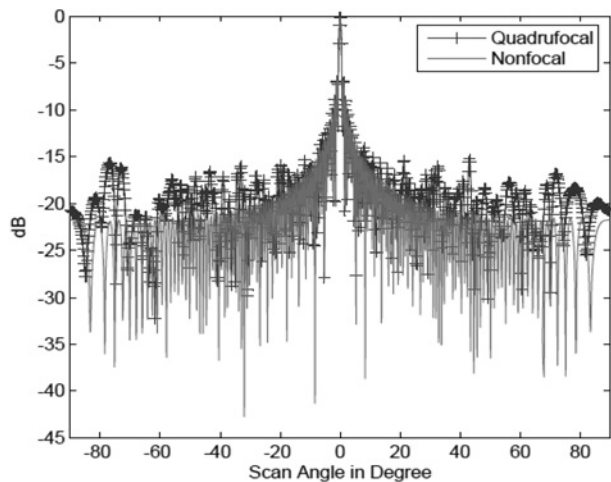


**Figure 9** Array factor comparison for quadrifocal and non-focal lenses at  $\alpha_i = 0^\circ$  for  $75\lambda$  aperture

adopted in this paper is affected by the number of variables, search region and convergence criteria. It is typically a random number, nevertheless, for a phase-error problem of (8) and (9), manageable in most personal computers nowadays. As an example, computation in Section 4 took only 1–2 min to converge in a computer with Pentium 1.6 GHz processor. Second, the general model in Fig. 4 considers all beam ports, receiving ports and transmission lines as design parameters. In practical formulation, however, this is not a necessary requirement. One can treat some of the design variables as priors, serving for certain special purposes. For instance, by confining the symmetry of beam and receiving contours and effectively interleaving the beam and receiving ports, a concept of a  $360^\circ$  scanning lens could be formulated, as shown in [21]. Third, it is worthwhile pointing out that in most practical Rotman lens designs, the structure initialisation always starts with one or more low phase-error models. After having these initial phase centres, different implementation methods, based on either microstrip, stripline or waveguide, follow different mechanism to locate the correct phase centre positions for the beam and receiving ports. Work proposed in this paper only serves the microstrip situation. Consequent research and rigorous mutual coupling studies can be performed using full-wave analyses.

## 5 Conclusions and future perspectives

In this paper we presented an alternative 2D Rotman lens design and optimisation technique. The proposed non-focal lens approach allows treating the beam port positions, inner receiving port positions, transmission lines and dielectric constants as the optimisation parameters. The degrees of freedom are usually confined by the path length equations in the conventional focal lens designs, which have been relaxed in the non-focal design. Typical 2D trifocal and quadrifocal lenses formulations and

optimisation concepts are reviewed. Good optimisation results based on non-focal scheme are demonstrated by comparing with the trifocal and quadrifocal Rotman lens designs. Phase error as well as array factor analysis show that the non-focal lens improvement becomes significant as the aperture size in wavelength grows in practical design.

## 6 References

- [1] ROTMAN W., TURNER R.: 'Wide-angle microwave lens for line source applications', *IEEE Trans. Antennas Propag.*, 1963, **11**, pp. 623–632
- [2] SMITH M.S.: 'Amplitude performance of Ruze and Rotman lenses', *Radio Electron*, 1983, **53**, pp. 329–336
- [3] PETERSON A.F., RAUSCH E.O.: 'Scattering matrix integral equation analysis for the design of a waveguide Rotman Lens', *IEEE Trans. Antennas Propag.*, 1999, **47**, pp. 870–878
- [4] KILIC O., DAHLSTROM R.: 'Rotman lens beam formers for army multifunction RF antenna applications'. *IEEE Antennas and Propagation Society Int. Symp.*, 2005, vol. 2B, pp. 43–46
- [5] WEISS S., DAHLSTROM R.: 'Rotman lens development at the army research lab'. *IEEE Aerospace Conf.*, 2006, p. 7
- [6] KATAGI T., MANO S., SATO S., TAHARA S., TOMIMATSU E.: 'an improved design method of Rotman lens antennas', *IEEE Trans. Antennas Propag.*, 1982, **20**, pp. 136–139
- [7] HANSEN R.C.: 'Design trades for Rotman lenses', *IEEE Trans. Antennas Propag.*, 1991, **39**, pp. 464–472
- [8] SMITH M.S.: 'Design considerations for Ruze and Rotman lens', *Radio Electron. Eng.*, 1982, **52**, pp. 181–187
- [9] RAPPAPORT C., ZAGHLOUL A.: 'Optimized three-dimensional lenses for wide-angle scanning', *IEEE Trans. Antennas Propag.*, 1985, **33**, pp. 1227–1236
- [10] MUSA L., SMITH M.: 'Microstrip Rotman lens port design'. *Antennas Propagation Society Int. Symp.*, 1986, pp. 899–902
- [11] MUSA L., SMITH M.S.: 'Microstrip port design and sidewall absorption for printed Rotman lenses', *IEE Proc. Microw. Antennas Propag.*, 1989, **136**, pp. 53–58
- [12] CRUZ B.G.J.L., NAVARRO E.A., SUCH V.: 'The phase center position of a microstrip horn radiating in an infinite parallel-plate waveguide', *IEEE Trans. Antennas Propag.*, 1994, **42**, p. 4
- [13] DONG J., ZAGHLOUL A.I., ROTMAN R.: 'A fast ray tracing method for microstrip Rotman lens analysis'. XXIXth URSI General Assembly, Chicago, 2008

- [14] MAYBELL M.: 'Ray structure method for coupling coefficient analysis of the two dimensional Rotman lens'. *Antennas and Propagation Society Int. Symp.*, 1981, pp. 144–147
- [15] RAO J.: 'Multifocal three-dimensional bootlace lenses', *IEEE Trans. Antennas Propag.*, 1982, **30**, pp. 1050–1056
- [16] GOLDBERG D.E.: 'Genetic algorithms in search, optimization and machine learning' (Kluwer Academic Publishers, Boston, MA, 1989)
- [17] SU D., DONG J., ZHENG Z.: 'A stochastic algorithm for function minimization', *Optim. Online*, 2008
- [18] ROTMAN R., ROTMAN S., ROTMAN W., RAZ O., TUR M.: 'Wideband RF beam-forming: the Rotman lens vs. photonic beam-forming'. *IEEE Antennas Propagation. Soc. Int. Symp.*, 2005, vol. 2B, pp. 23–26
- [19] DONG J., ZAGHLOUL A.I., SUN R., REDDY C.J.: 'EHF Rotman lens for electronic scanning antennas'. *Asia Pacific Microwave Conf.*, Hong Kong, 2008
- [20] CLARK S., MARTIN C., KOLINKO V., LOVBERG J., COSTIANES P.J.: 'A real-time wide field of view passive millimeter-wave imaging camera'. *Proc. 32nd Applied Imagery Pattern Recognition Workshop*, Washington, DC, 2003, pp. 250–254
- [21] ZAGHLOUL A.I., DONG J.: 'A concept for a lens configuration for 360° scanning', *IEEE Antennas Wirel. Propag. Lett.*, 2009, **8**, pp. 985–988